MNRAS 000, 1–14 (2020) Preprint 4 February 2021 Compiled using MNRAS LATEX style file v3.0

Orphan galaxies in semi-analytic models

Facundo M. Delfino,[1,2]★ Claudia G. Scóccola,[1,2] Sofía A. Cora[1,2,3], Cristian A. Vega-Martinez[4,5] and Ignacio D. Gargiulo[2,3]

[1] *Facultad de Ciencias Astronómicas y Geofísicas, Universidad Nacional de La Plata, Observatorio Astronómico, Paseo del Bosque, B1900FWA La Plata, Argentina*

[2] *Consejo Nacional de Investigaciones Científicas y Técnicas (CONICET), Rivadavia 1917, Buenos Aires, Argentina,*

[3] *Instituto de Astrofísica de La Plata (CCT La Plata, CONICET, UNLP), Observatorio Astronómico, Paseo del Bosque B1900FWA, La Plata, Argentina,*

[4] *Instituto de Investigación Multidisciplinar en Ciencia y Tecnología, Universidad de La Serena, Raúl Bitrán 1305, La Serena, Chile,*

[5] *Departamento de Astronomía, Universidad de La Serena, Av. Juan Cisternas 1200 Norte, La Serena, Chile*

Accepted XXX. Received YYY; in original form ZZZ

ABSTRACT

We present an updated model for the evolution of the orbits of "orphan galaxies" to be used in the SAG semi-analytical model of galaxy formation and evolution. In cosmological simulations, orphan galaxies are those satellite galaxies for which, due to limited mass resolution, halo finders lose track of their dark matter subhalos and can no longer be distinguished as self-bound overdensities within the larger host system. Since the evolution of orphans depends strongly on the orbit they describe within their host halo, a proper treatment of their evolution is crucial in predicting the distribution of subhalos and satellite galaxies. The model proposed takes into account the dynamical friction drag, mass loss by tidal stripping and a proximity merger criterion, also it is simple enough to be inexpensive from a computational point of view. To calibrate this model, we apply it onto a dark matter only simulation and compare the results with a high resolution simulation, considering the halo mass function and the two-point correlation function as constraints. We show that while the halo mass function fails to put tight constraints on the dynamical friction, the addition of clustering information helps to better define the parameters of the model related to the spatial distribution of subhalos. Using the model with the best fit parameters allows us to reproduce the halo mass function to a precision better than 5 per cent, and the two point correlation function at a precision better than 10 per cent.

Key words: galaxies:formation – galaxies:evolution – galaxies: haloes – methods: numerical

1 INTRODUCTION

The observed Universe is successfully described by the ΛCDM model. According to this concordance model, at early times, the Universe underwent a period of exponential expansion, called Inflation, in which the primordial perturbations in the metric were settled. These metric fluctuations produced perturbations in the matter density field that are characterised by the matter power spectrum. The large scale structure (LSS) we see today is the result of the gravitational growth of these tiny matter perturbations. It is currently accepted that structure formation proceeds in a hierarchical way, with small structures being the first ones to collapse and reach a state close to virial equilibrium. Larger structures, like massive dark matter (DM) haloes, form later by mergers of pre-existing virialised haloes, and by accretion of diffuse dark matter (Frenk & White 2012). Within the dark matter haloes, the first galaxies are born and evolve (White & Rees 1978).

Galaxies are highly non-linear objects that are the result of a complex formation mechanism, which involves several astrophysical processes and spans a wide range of spatial scales (for a review of the theory of galaxy formation and evolution see, e.g. Benson 2010; Silk & Mamon 2012; Wechsler & Tinker 2018). Due to the non-linear nature of these processes, it is not feasible to treat them using analytic methods and hence the use of N-body simulations is required. The most common approaches to generate simulated galaxy populations are *Hydrodynamic Simulations*, *Halo Occupation Distributions* and *Semi-Analytic Models*, each of them having advantages and disadvantages (see e.g. Vogelsberger et al. 2020).

On large scales, hydrodynamic simulations can take into account the effects of both dark matter content and baryons. However, for scales below the resolution limit of the grid, the astrophysical processes are simulated using semi-analytic recipes. Since the number of physical processes to be solved is very large, these simulations are usually extremely demanding on computing power. At present, the state-of-the-art of this class of simulations corresponds to the Virgo Consortium's EAGLE project (Schaye et al. 2015; Crain et al. 2015) and The Next Generation Illustris project (IllustrisTNG, Springel et al. 2018; Nelson et al. 2018; Pillepich et al.

★ E-mail: fdelfino@fcaglp.unlp.edu.ar

2018; Naiman et al. 2018; Marinacci et al. 2018). Although these simulations have very high resolution, the main disadvantage is that their volumes are small compared to actual real galaxy surveys such as eBOSS (Dawson et al. 2015, 2016; eBOSS Collaboration et al. 2020), LSST (LSST Science Collaboration et al. 2009; LSST Dark Energy Science Collaboration 2012; The LSST Dark Energy Science Collaboration et al. 2018), DESI (Levi et al. 2013; DESI Collaboration et al. 2016) or Euclid (Laureijs et al. 2011; Amendola et al. 2013; Euclid Collaboration et al. 2019).

On the other hand, there are methods that aim at populating dark matter haloes obtained in N-body simulations with galaxies. For example, the Halo Occupation Distribution (HOD, e.g Peacock & Smith 2000; Berlind & Weinberg 2002; Berlind et al. 2003) method describes the abundance of galaxies inside a given halo as a parametric function of the host halo mass. Another popular statistical method is the Sub-Halo Abundance Matching (SHAM, e.g. Kravtsov et al. 2004; Vale & Ostriker 2004; Conroy et al. 2006; Behroozi et al. 2010; Moster et al. 2010; Trujillo-Gomez et al. 2011; Reddick et al. 2013), where the most massive/luminous galaxies are assigned to the most massive subhaloes. These methods are relatively easy to implement and with them, we are able to obtain large-volume galaxy catalogues at a low computational cost. However, it remains difficult to move from this statistical characterisation of the connection between dark matter haloes and galaxies to a physical understanding of the galaxy formation process.

Semi-analytic models (SAMs, e.g. Springel et al. 2001b; Croton et al. 2006; Cora 2006; Benson 2012; Henriques et al. 2013; Gonzalez-Perez et al. 2014) are a good alternative to overcome the disadvantages of the previous methods. These models populate dark matter haloes with simulated galaxies, where the physical processes related to their formation and evolution are treated using semi-analytic approximations. Due to their flexibility, large dynamical range in mass and spatial resolution, and relatively low computational costs, semi-analytic models represent an ideal tool to build simulated galaxy populations in cosmological volumes. In addition, they enable to test the physical processes that determine the evolution of galaxies. For a review of semi-analytic methods see Baugh (2006).

As said before, structure formation in the Universe is a hierarchical process, in which the first galaxies are formed in the potential wells generated by dark matter haloes. Then, as the Universe evolves, accretions between halos that host galaxies may occur. In that case, the most massive galaxy occupies the centre of the new halo while the least massive ones become satellite galaxies. A satellite halo orbiting within its main system loses mass by tidal stripping and experiences dynamical friction, a drag force that gradually shrinks its orbit until it eventually merges with the central galaxy. On the other hand, in dark matter simulations, it may occur that the halo finder algorithm loses track of a subhalo when it can no longer be distinguished as a self-bound overdensity within the host system. Satellite galaxies that have lost their dark matter subhalo, either by a merger with a larger structure or by artificial disruptions, and still persist in the simulation are called "orphan galaxies".

The evolution of satellite galaxies depends strongly on the orbit they describe within their host halo (see e.g. Vollmer et al. 2001). For example, a satellite halo orbiting within its host is subjected to tidal forces that cause the satellite galaxy to lose mass via tidal stripping (TS) mechanism. TS depends strongly on the circularization of the orbit, where most of the mass (DM of the satellite halo, and gas mass and stellar mass of the satellite galaxy) is lost when the halo passes through the pericentre. Also, tidal shocks at the pericentres of the orbit increase the kinetic energy and the satellite halo expands (*tidal heating*), making it more susceptible to tidal stripping (Zentner & Bullock 2003; Gan et al. 2010; Pullen et al. 2014). Ram pressure stripping (RPS, Gunn & Gott 1972) is another mechanism that produces material loss, affecting only the gas content of the satellite galaxy that moves within a high density environment. Indeed, a galaxy that moves in an eccentric orbit experiences periods of strong RPS as it approaches the pericentre combined with periods of low RPS as it passes through the apocentre. On the other hand, a slowly decaying galaxy will experience a continuous increase in RPS as it falls into denser regions (Brüggen & De Lucia 2007). All these processes depend on the position and velocities of satellite galaxies, so a proper treatment of orphan satellite orbits is crucial.

In this work, we present an updated treatment for the orbits of orphan satellite galaxies used in the semi-analytic model SAG (Semi-Analytic Galaxies, Cora 2006; Lagos et al. 2008; Tecce et al. 2010; Orsi et al. 2014; Muñoz Arancibia et al. 2015; Gargiulo et al. 2015; Cora et al. 2018). In the previous version of SAG, when a subhalo is no longer identified due to a merger with a larger structure, its corresponding galaxy becomes an orphan. Assuming a circular orbit, the orphan is initially located at a distance of its host given by the virial radius and with a velocity determined by the virial velocity of the host. The evolution of the radial distance is estimated using dynamical friction, with randomly generated positions and velocities. Finally, the orphan merges with the central galaxy in a time according to the dynamical friction time-scale (Pujol et al. 2017). Here we present an improved model for the evolution of orphan galaxies which includes analytic prescriptions for the tidal stripping (TS) and dynamical friction (DF) mechanisms.

Using different SAM and HOD models, Pujol et al. (2017) studied the impact that different orphan satellite treatments have on the clustering signal. In general, it is found that models that do not include orphans present a lower clustering at low scales. This result is consistent with the work of Kitzbichler & White (2008). These authors use a SAM model to show that, without the addition of orphan satellites, the clustering at low scales is much lower than that observed in actual galaxy surveys. In addition, Guo & White (2014) show that the inclusion of orphan satellites improves the abundance of subhaloes at low masses and removes the resolution dependence observed between SHAM catalogues built from simulations of different resolutions. Based on these results, we propose to apply the orphan evolution model to a dark matter only simulation, and compare the results to a higher resolution simulation with the same settings, considering the halo mass function and the two-point correlation function as constraining relations. In the higher resolution simulation, there are subhaloes that would not be identified by the halo finder algorithm in the lower resolution simulation. We assume that the difference in those constraining relations will be given by the orphan galaxies, and use these quantities to tune the parameters of the orbit model.

Finally, it is important to remark that, in this study, we only consider DM subhalos and in no case do we apply the semi-analytical model. Therefore, when we refer to "orphan galaxies", "orphan satellites" or simply "orphans", we always refer to the subhalos corresponding to orphan galaxies and not to the orphan galaxies themselves.

This paper is organised as follows: in Section 2, we introduce the orbit model for the orphan galaxies and its many ingredients. Section 3 describes the statistical tools used to analyse galaxy clustering and gives details about the simulations used in this work, MDPL2 and SMDPL. In Section 4, we describe the method used to calibrate the free parameters of the model and discuss our results in Section 5. We present our conclusions in Section 6.

2 EVOLUTION MODEL FOR ORPHAN GALAXIES

As many other SAMs, the SAG model of galaxy formation and evolution takes as input the properties of dark matter haloes and their merger trees extracted from cosmological N-body simulations (see e.g. Roukema et al. 1997; Springel et al. 2001b; Croton et al. 2006). Based on this information, the model assigns a central galaxy to each new halo that appears in the simulation and then simulates its evolution. The central galaxies of main halos are referred to as *type 0* galaxies, while the central galaxies of satellite halos are labelled as *type 1*. Finally, orphan galaxies (i. e. galaxies that have lost their host halo) are referred to as *type 2* galaxies. For type 0 and type 1 galaxies, where the halo finder is still able to identify their dark matter haloes, effects such as dynamical friction or tidal stripping are given in a self-consistent way by the base N-body simulation. On the other hand, for type 2 (orphans) galaxies, since they lose their DM halo, we cannot follow their evolution. To avoid this problem, when a subhalo is no longer detected by the halo finder algorithm, the model continues integrating its orbit numerically, taking as initial conditions the position, velocity, mass and radius of the halo at the instant of last identification, as given by the N-body simulation.

The simplest model of a subhalo moving within its host halo can be approximated by a point mass without internal structure orbiting in a static potential. This model does not take into account important aspects of the composition and evolution of satellite haloes such as the internal structure of the subhalo or the interactions with the material that forms the host halo. For example, the interaction between the subhalo and the matter of its host gives rise to a dynamical friction force that causes the evolution of the orbits to deviate from that of the simplest model. In addition, during their evolution, satellite haloes may experience mass loss due to tidal stripping mechanism or gravitational shocks. Therefore, to describe the subhalo evolution accurately, it is necessary to take into account all the processes mentioned above.

Within our semi-analytic model SAG, we consider each orphan galaxy as a particle whose properties may change over time. The orbits of this type of satellite galaxies are estimated in a pre-processing step, that is, before applying SAG to the underlying cosmological DM simulation. To determine the orbit of an orphan galaxy, we consider each subhalo as a particle of the same mass moving in a smooth spherical potential generated by its host halo. In order to take into account the effect of the host halo over the satellite, at each instant, we compute the effect of dynamical friction using Chandrasekhar's formula and we also take into account the loss of material by considering a tidal stripping model. If the mass of a subhalo falls below a certain resolution limit we consider it disrupted; if, at any instant, the satellite-host distance is less than a fraction of the viral radius of the host we consider the satellite galaxy to be merged with its host. Below, we describe these processes in more detail.

2.1 Dynamical friction (DF)

When a subhalo of total mass $M_{\rm sat}$ moves through a large collisionless system composed of particles of mass $m << M_{\rm sat}$, it perturbs the particle field creating an over-dense region behind it. This "wake" pulls the subhalo in the opposite direction causing a drag force called *dynamical friction*. Therefore, we can separate the force experienced by an orphan galaxy orbiting within a massive halo into two contributions: one due to the potential of the central halo, and a higher-order correction due to the background particles (the dynamical friction term). The first part is given by the simple expression $f_i = -\partial\Phi/\partial x_i$, that relates the force acting on a particle at a given position with the potential of the main system Φ at that position. The dynamical friction force is given by the Chandrasekhar formula (Chandrasekhar 1943; Binney & Tremaine 2008), i. e.

$$\mathbf{F}_{\rm df}(r) = -\frac{4\pi G^2 M_{\rm sat}^2 \rho_{\rm host}(r) \ln\Lambda}{V^2}\left[\mathrm{erf}(X) - \frac{2X}{\sqrt{\pi}}\exp(-X^2)\right]\frac{\mathbf{V}}{V}\,, \tag{1}$$

where r is the position of the satellite relative to its host halo, $\mathbf{V}$ is the subhalo velocity, $V = |\mathbf{V}|$, $X = V/(\sqrt{2}\sigma)$ with σ the velocity dispersion of dark matter particles, $\rho_{\rm host}$ represents the density distribution of the host halo, $\ln\Lambda$ is the Coulomb logarithm and erf is the Gauss error function.

Assuming a NFW profile (Navarro et al. 1997) for the density distribution $\rho_{\rm host}$ and an isotropic velocity distribution, the velocity dispersion σ is given by Łokas & Mamon (2001)

$$\frac{\sigma^2(s)}{V_{\rm vir}^2} = g(c)s(1+cs)^2\int_s^\infty\left[\frac{1}{g(cs)s^3(1+cs)^2}\right]ds\,, \tag{2}$$

where c is the concentration parameter, $1/g(x) = \log(1+x) - x/(1+x)$, and s is the distance normalised by the virial radius. Further details on the NFW density profile can be found in Appendix A and in Łokas & Mamon (2001). For simplicity, in this work we use the following approximation for σ, which is accurate to 1 per cent for x in the range $0.01 - 100$ (Zentner & Bullock 2003)

$$\sigma(x) \simeq V_{\rm max}\frac{1.4393\,x^{-0.354}}{1 + 1.1756\,x^{-0.725}}\,, \tag{3}$$

where $x = cs$, and $V_{\rm max}$ is the maximum circular velocity related to the virial velocity via $V_{\rm max} \simeq V_{\rm vir}\sqrt{0.216\,c\,g(c)}$.

The argument of the Coulomb logarithm can be expressed as $\Lambda = b_{\rm max}/b_{\rm min}$ where $b_{\rm max}$ and $b_{\rm min}$ are the maximum and the minimum impact parameters for gravitational encounters between the satellite and the background objects (Binney & Tremaine 2008). Typically, $b_{\rm min}$ corresponds to a close encounter, then $b_{\rm min} \simeq GM_{\rm sat}/V^2$ where V is a velocity typical of the encounter, such as the rms velocity of the background particles. The choice of the value for $b_{\rm max}$ is more ambiguous, and for a finite system is taken to be the characteristic scale of the system.

It should be noted that the derivation of Chandrasekhar's formula assumes a massive particle moving in a homogeneous medium composed by an infinite number of low-mass particles with a Maxwellian velocity distribution. However, in the literature, several works show that this equation is applicable to more general contexts, where these hypotheses are not satisfied, if the Coulomb logarithm is chosen appropriately (Weinberg 1986; Cora et al. 1997; Velazquez & White 1999).

There has been much debate in the literature about the appropriate choice of Coulomb logarithm. For example, Springel et al. (2001b) uses an approach given by $\ln\Lambda \simeq \ln(1 + M_{\rm cen}/M_{\rm sat})$ where $M_{\rm cen}$ and $M_{\rm sat}$ are the masses of the central halo and the satellite subhalo, respectively. On the other hand, some authors use other definitions that allow them to reproduce results from N-body simulations (Hashimoto et al. 2003; Zentner & Bullock 2003; Petts et al. 2015, 2016; Ogiya & Burkert 2016). In particular, Hashimoto et al. (2003), hereafter H03, propose a variable Coulomb logarithm. This choice avoids the strong circularization effect that is observed when

comparing these models with the results obtained from N-body simulations. Following this, we use the expression

$$\ln \Lambda = \begin{cases} \ln(r/bR_{\rm sat}) & r > bR_{\rm sat} \\ 0 & r \leq bR_{\rm sat} \end{cases} , \tag{4}$$

where r is the distance from the satellite subhalo to the centre of the host halo, $R_{\rm sat}$ is the virial radius of the satellite and b is a free parameter. Note that in H03, the Coulomb logarithm is given by $\ln \Lambda = \ln(r/1.4\epsilon_{\rm sat})$ for $r > 1.4\epsilon_{\rm sat}$, where $\epsilon_{\rm sat}$ is the softening length corresponding to a Plummer sphere. Here we assume a NFW profile for the satellite, thus we introduce the virial radius of the subhalo and leave b as a free parameter to be adjusted.

2.2 Tidal stripping (TS)

As mentioned above, a subhalo orbiting within its host system is subjected to tidal forces. When tidal forces are greater than the gravitational force of the satellite itself, the material becomes unbound and the satellite loses mass. The dynamical friction force is proportional to $M_{\rm sat}^2$ (see equation 1), and hence the magnitude of the deceleration experienced by a satellite halo is proportional to $M_{\rm sat}$. As a result, mass loss can have a major impact on the orbital evolution of the satellite halo. For this reason, it is necessary to estimate the amount of mass lost by tidal stripping.

We estimate the tidal radius as the distance at which the self-gravity force and the tidal forces cancel out; material outside this distance become unbound and could be stripped out from the satellite. The tidal radius is given by

$$r_{\rm t} = \left(\frac{GM_{\rm sat}}{\omega^2 - d^2\Phi/dr^2} \right)^{1/3} , \tag{5}$$

where $M_{\rm sat}$ is the mass of the satellite, ω is its angular velocity and Φ characterise the potential of the host system (King 1962; Taylor & Babul 2001; Zentner & Bullock 2003). This equation is derived under the assumption that the satellite moves in a circular orbit and the potential of the main system is spherically symmetric. But, even under these restricted assumptions, the tidal limit cannot be represented as a spherical surface, because some particles of the satellite within $r_{\rm t}$ are unbound while other particles outside $r_{\rm t}$ may remain bound to the suhalo (Binney & Tremaine 2008).

In general, satellites do not move in circular orbits and the potential of the host system is not spherically symmetric. As an approximation, we can still apply equation 5 to eccentric orbits, in which case we estimate an instantaneous tidal radius by using the corresponding instantaneous values, i.e. $\omega = |\mathbf{V} \times \mathbf{r}|/r^2$, where $\mathbf{V}$ and $\mathbf{r}$ are the instantaneous position and velocity of the subhalo. Another aspect that remains unclear is the rate at which the material located outside the instantaneous tidal radius $r_{\rm t}$ is going to be removed. Following Zentner et al. (2005), we absorb all these complicated details in a free parameter to be adjusted by external constraints. Then, the rate of mass loss of the satellite subhalo by TS is given by

$$\frac{dM_{\rm sat}}{dt} = -\alpha \frac{M_{\rm sat}(> r_{\rm t})}{T_{\rm orb}} . \tag{6}$$

Here $T_{\rm orb} = 2\pi/\omega$, with ω the instantaneous angular velocity of the satellite, and α is treated as a free parameter. The value of the parameter α differs from author to author. For example, Taylor & Babul (2001) and Zentner & Bullock (2003) choose a value $\alpha = 1$; on the other hand, Peñarrubia & Benson (2005) assume an instantaneous stripping , which effectively implies $\alpha \to \infty$. Finally, some authors (e.g. Zentner et al. 2005, Pullen et al. 2014) vary the value of α in order to reproduce the halo mass function of simulations. In this paper, we will follow the latter approach.

2.3 Merger criterion

According to hierarchical structure formation models, mergers play a critical role in the formation and evolution of galaxies. Thus, a criterion to determine whether an orphan satellite is merged with its host is another important aspect to take into account. In the case of type 2 galaxies, since the halo finder cannot follow its evolution, if we want to estimate the time that orphan satellites remain in the simulation before merging we need to rely on alternative methods.

One possibility, is to use an analytical expression to estimate this using a dynamical friction timescale $t_{\rm df}$ (Binney & Tremaine 2008). Then, an orphan satellite galaxy remains in the simulation as long as the time it has orbited around its central galaxy is less than $t_{\rm df}$. Instead of using an analytical estimate, in this paper, following (Boylan-Kolchin et al. 2008), we assume that a subhalo that is not longer detected (and its corresponding galaxy) merges with its host halo when it loses 99 percent of its initial angular momentum. When that condition is satisfied, the subhalo is considered merged. In addition to this condition on angular momentum, we will also define a proximity criterion for mergers: we consider a subhalo to be merged when the subhalo-host distance is smaller than a fraction f of the virial radius of the main system; i.e. if

$$r_{\rm sat} < f R_{\rm host} , \tag{7}$$

where we treat f as a free parameter of the model. Therefore, we consider a subhalo to be merged with its host halo when any of the above criteria is met; either the subhalo loses 99 percent of its initial angular momentum, or it gets very close to the centre of the host halo, as determined by equation 7.

2.4 Implementation of the model

Once the subhalo of a galaxy is no longer detected by the halo finder algorithm, we cannot follow its position evolution and we flag it as a type 2 galaxy (orphan). From that moment on, we integrate its orbit numerically taking as initial conditions the last known values of position, velocity, mass and radius. The subhalo orbit between two snapshots is divided into time intervals of length δt. Here, the time spacing between snapshots is given by the base DM simulation. At each time interval, we compute the forces that act over the subhalo according to equations 1, 3 and 4, and perform the evolution of positions and velocities using a kick-drift-kick (KDK) leapfrog scheme.

Between snapshots, we took outputs of the orbit evolution of the subhalo at time intervals given by Δt ($\Delta t > \delta t$). For each output we compute the tidal radius $r_{\rm t}$ (equation 5). If $r_{\rm t}$ is smaller than the current radius of the subhalo, we assume that a certain amount of material that is outside $r_{\rm t}$ is unbound and can be removed by tidal stripping. At this stage, we remove an amount of material equivalent to $\Delta t/T_{\rm strip} = \alpha \Delta t/T_{\rm orb}$ from the unbound mass, that is

$$\Delta M_{\rm sat} = \alpha M_{\rm sat}(r > r_{\rm t}) \frac{\Delta t}{T_{\rm orb}} \tag{8}$$

where $M_{\rm sat}(r > r_{\rm t})$ is the mass of the satellite outside a radius $r_{\rm t}$

and $T_{\rm orb}$ is the same as in equation 6. Then, we update the mass and radius to the new values. In this procedure, we assume that the original density profile is not altered by the stripping process. No stripping takes place if $r_{\rm t}$ is greater than the original radius of the satellite halo. We continue evolving the subhalo of an orphan galaxy until a merger with its host eventually occurs, following the criteria explained in the previous subsection (see equation 7). If the subhalo mass is reduced below a threshold limit, the satellite is considered disrupted.

3 METHODOLOGY

In the previous section, we introduced a model for the evolution of the orbits of orphan galaxies in SAG. This model depends on free parameters that have to be determined by external constraints. In this work, we propose to use the halo mass function (HMF) and the two-point correlation function (2PCF) as constraints for the free parameters of the orbit model, (b, f, α), introduced in equations 4, 6 and 7, respectively.

We apply our model to two dark matter only N-body simulations, with the same cosmological parameters but different mass and force resolutions. It is worth noting that in the higher resolution simulation, the majority of halos that disappear in the lower resolution simulation, leaving an orphan galaxy, will be detected by the halo finder. The results of the orbit model applied to the low resolution simulation can be compared with those obtained from the high resolution one, which is considered as the reference simulation. Then, we vary the free parameters of the model, until we find a combination for which the low resolution simulation converges to the high resolution one, both for the halo mass function ($\phi = dn/d\log M$, with n the numerical density) and for the two-point correlation function (ξ).

Below, we describe the set of dark matter only simulations used in this work and the computation of the 2PCF. In order to find optimal parameter values, we need to run the model several times. Since running the code over the full boxes is a numerically expensive task, we make a parameter exploration over a set of calibration boxes, which are selected subvolumes of the full simulations with 2PCF and HMF similar to those of the full boxes. The details of this procedure is covered in the rest of this section.

3.1 MDPL2 and SMDPL simulations

In this subsection, we describe the two N-body simulations with different mass and force resolutions that we use for our study of the evolution of the orbits of orphan satellites. SMDPL and MDPL2 are dark matter only N-body simulations that are part of the MultiDark cosmological simulation suite[1]. These simulations follow the evolution of 3840^3 particles within a box, and are characterised by Planck cosmological parameters: $\Omega_{\rm m} = 0.307$, $\Omega_\Lambda = 0.693$, $\Omega_{\rm b} = 0.048$, $n_{\rm s} = 0.96$ and $H_0 = 100\ h\,{\rm km\,s^{-1}\,Mpc^{-1}}$, where $h = 0.678$ (Planck Collaboration et al. 2016). Both simulations have been carried out with L-GADGET-2 code, a version of the publicly available code GADGET-2 (Springel et al. 2001a; Springel 2005) whose performance has been optimised for simulating large numbers of particles. SMDPL simulation has a box size of 400 h^{-1} Mpc which implies a particle mass of $9.6 \times 10^7\ h^{-1}\,{\rm M}_\odot$, while MDPL2 simulation has a box size of 1 h^{-1} Gpc which implies dark matter particles of $1.5 \times 10^9\ h^{-1}\,{\rm M}_\odot$. Table 1 shows the numerical and cosmological parameters for the simulations. For more details about this set of cosmological simulations see Klypin et al. (2016).

These simulations were analysed with the ROCKSTAR halo finder (Behroozi et al. 2013a), and merger trees were constructed using CONSISTENT-TREES (Behroozi et al. 2013b). The virial mass of these structures is defined as the mass enclosed by a sphere of radius $R_{\rm vir}$, so that the mean density is equal to $\Delta = 200$ times the critical density of the universe $\rho_{\rm c}$, i.e. $M_{\rm vir} = 4/3\pi R_{\rm vir}^3 \Delta\rho_{\rm c}$. Dark matter haloes can exist over the background density or lie within another dark matter halo. To differentiate them, the former are referred to as main host haloes, whereas the latter are called subhaloes or satellite haloes.

Figure 1 shows the HMF of the full sample of haloes for the SMDPL ($\phi_{\rm SM}$ in solid line) and MDPL2 ($\phi_{\rm MD}$ in dashed line) simulations at redshift $z = 0$. The halo mass function for the MDPL2 simulation presents a break at a mass of $\sim 10^{10.4}\ h^{-1}\,{\rm M}_\odot$, which establishes the minimum mass from which we can guarantee that we have completeness in the number of haloes for both simulations (vertical dashed line in Figure 1). In the lower panel, the fractional difference between the HMF of the MDPL2 simulation with respect to the one of the SMDPL simulation is shown. In the mass range $10^{10.4} - 10^{11.0}\ h^{-1}\,{\rm M}_\odot$, the fractional difference is of the order of 0.2, hence there are 20 percent more low mass haloes in SMDPL as compared to MDPL2. On the other hand, for halo masses greater than $10^{11.4}\ h^{-1}\,{\rm M}_\odot$, the fractional difference is always below 0.05 (horizontal dashed line). This shows that concerning halo mass functions, the difference between SMDPL and MDPL2 is within the calibration specification (5 per cent) obtained by Tinker et al. (2008) (see also Behroozi et al. 2013a).

The ROCKSTAR halo finder considers groups formed by at least ten dark matter particles, although halo properties are not robust when approaching this minimum. According to Behroozi et al. (2013a), halo detection is reliable for structures composed of at least twenty dark matter particles. For a minimum of ten particles, a simple calculation tells us that the minimum detected halo mass for MDPL2 is $\sim 10^{10.2}\ h^{-1}\,{\rm M}_\odot$, while this calculation for SMDPL gives a minimum halo mass of $\sim 10^9\ h^{-1}\,{\rm M}_\odot$. Since completeness is important when comparing the two point correlation functions of different simulations, in this paper we will consider only haloes with masses greater than $10^{10.4}\ h^{-1}\,{\rm M}_\odot$ for both simulations (see vertical dashed line in Figure 1).

3.2 The two-point correlation function

Given a set of points, the probability of finding an object in an infinitesimal volume dV is, $dP = ndV$, where n is the mean number density and $N = nV$ is the number of objects in a finite volume V. Then, the 2PCF is defined as the excess probability of finding one of them inside a small volume dV_1 and the other in a small volume dV_2, separated by a distance r (Peebles 1980; Martínez & Saar 2001)

$$dP = n^2(1 + \xi(r))dV_1 dV_2. \tag{9}$$

In practice, for a catalogue of N particles and volume V with periodic boundary conditions, the 2PCF can be estimated by counting the number of pairs of objects, $N_{\rm s}(r)$, in a shell of volume, $V_{\rm s}(r)$, at distance r from each other using

$$\xi(r) = \frac{1}{n^2 V}\frac{N_{\rm s}(r)}{V_{\rm s}(r)} - 1. \tag{10}$$

[1] https://www.cosmosim.org/

simulation	box h^{-1} Gpc	N_p	m_p h^{-1} M$_\odot$	ϵ h^{-1} kpc	Ω_m	Ω_b	Ω_Λ	σ_8	n_s	H_0 km s^{-1} Mpc^{-1}
MDPL2	1.0	3830^3	1.5×10^9	5.0	0.307	0.048	0.693	0.829	0.96	67.8
SMDPL	0.4	3830^3	9.6×10^7	1.5	0.307	0.048	0.693	0.829	0.96	67.8

Table 1. Numerical and cosmological parameters for the N-body simulations.

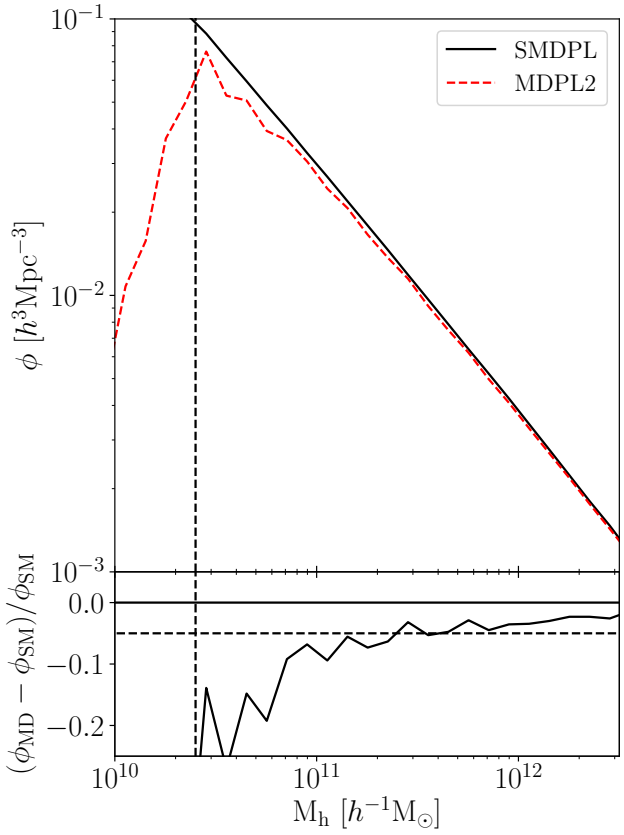

Figure 1. *Upper panel:* Halo mass function of MDPL2 (red dashed line) and SMDPL (black solid line) simulations for redshift $z = 0$. The vertical line denotes halo masses of $10^{10.4}$ h^{-1} M$_\odot$. Note that for masses below this limit, MDPL2 simulation presents a break which establishes the minimum mass from which we can guarantee that we have completeness in the number of haloes for both simulations. *Lower panel:* Fractional difference between MDPL2 and SMDPL halo mass functions. The dashed horizontal line indicates a fractional difference of 0.05. Note that for masses below than 10^{11} h^{-1} M$_\odot$ we have approximately 20 percent more haloes in SMDPL than in MDPL2.

However, if the boundaries are not periodic, this equation cannot be applied. This is the case for a real survey, or when we restrict the analysis to a small region within a large periodic simulation. In these cases, the common method consists in comparing the observed data (D), with catalogues composed of random points (R) that reproduce the same geometry and artefacts of the original catalogue. In general, random catalogues contain at least 10 times more objects than the data catalogue, in order to reduce the noise level. In such cases, the 2PCF can be computed using the Landy-Szalay estimator (Landy & Szalay 1993)

$$\xi(r) = \frac{DD(r) - 2DR(r) + RR(r)}{RR(r)}; \tag{11}$$

here $DD(r)$, $DR(r)$ and $RR(r)$ are the normalized data-data, data-random and random-random pairs, respectively. If N_d and N_r are the number of objects in D and R then

$$DD(r) = \frac{dd(r)}{N_d(N_d - 1)/2}, \tag{12}$$

$$RR(r) = \frac{rr(r)}{N_r(N_r - 1)/2}, \tag{13}$$

$$DR(r) = \frac{dr(r)}{N_d N_r}, \tag{14}$$

where $dd(r)$ is the number of objects pairs separated by a distance r in D, $rr(r)$ is the number of pairs separated by a distance r in R and $DR(r)$ is the cross-correlation statistic, the number of pairs separated by a distance r with one point taken from D and the other from R (for more details see e.g. Vargas-Magaña et al. 2013). To compute correlation functions, throughout this work we use the publicly available PYTHON package CORRFUNC (Sinha & Garrison 2020).

Figure 2 shows the 2PCF for halo masses greater than $10^{10.4}$ h^{-1} M$_\odot$ for the SMDPL (solid line) and MDPL2 (dashed line) simulations at redshift $z = 0$. From this figure, we see that the clustering of SMDPL is greater than that of MDPL2 for all scales, this effect is more significant at lower scales (between 0.01−0.1 h^{-1} Mpc). The suppression observed in the amplitude of the correlation function of MDPL2 could be due to a low force resolution. In cosmological simulations, the resolution of the gravitational force is defined by the value of the softening length ϵ. However, there are studies (see e.g. Jenkins et al. 1998) that show that the softening length introduces considerable suppression on the clustering signal only for separations lower than 2ϵ. In our case, MDPL2 is characterised by $\epsilon = 0.005$ h^{-1} Mpc, then for scales greater than 0.01 h^{-1} Mpc the effect of the softening length should be very small. Thus, the softening length can not account for the large clustering suppression seen in MDPL2 simulation for separations between $10^{-2} - 10^{-1}$ h^{-1} Mpc.

According to the halo model, the two-point correlation function can be decomposed into two contributions: a 1-halo term and a 2-halo term. The 1-halo term involves correlations between haloes belonging to the same system, i.e. correlations between central haloes and their corresponding satellites and correlations between all satellites that belong to a system. On the other hand, the 2-halo term involves correlations between haloes belonging to different systems (Cooray & Sheth 2002). When the contributions from these two terms are added together, the resulting correlation function should roughly follow a power law (see eg. Coil 2013). In general, the 2-halo term dominates at large scales (greater than 1 h^{-1} Mpc), while the 1-halo term dominates at scales lower than 1 h^{-1} Mpc. Note that the characteristic scale $\sim$ 1 h^{-1} Mpc, which is of the order of the size of the main systems, indicates the transition between the two regimes. In van den Bosch et al. (2013), it is shown that increasing the number of satellites increases mainly the 1-halo term,

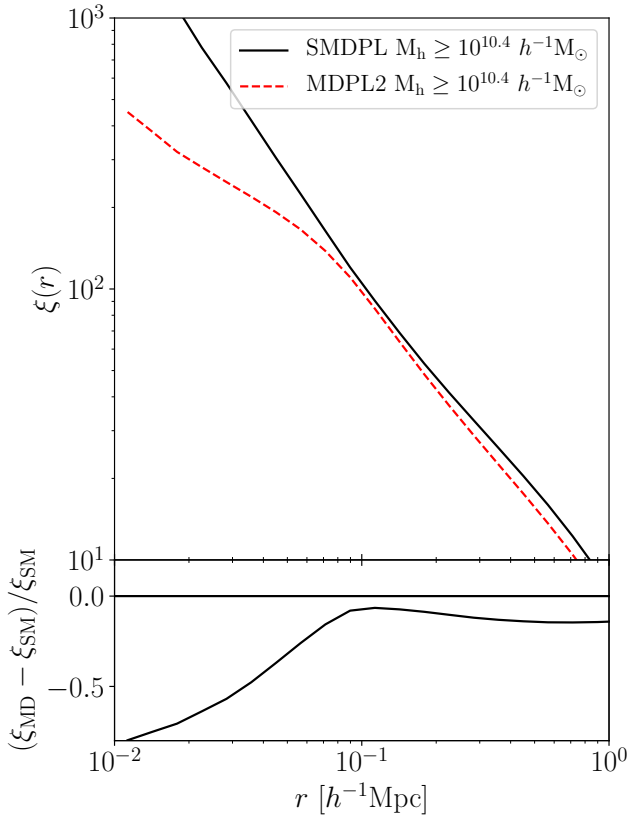

Figure 2. *Upper panel:* Two-point correlation function for the SMDPL (black solid line) and MDPL2 (red dashed line) simulations at redshift $z = 0$. *Lower panel:* The fractional difference between MDPL2 and SMDPL two-point correlation functions. For separations greater than 0.1 h^{-1} Mpc, both simulations present a similar clustering. However, for smaller scales, the clustering functions differ considerably (fractional difference is greater than 0.5 for scales close to 0.01). The lower satellite fraction in MDPL2 compared to the one in SMDPL, implies a lower number of pairs at low scales (where the 1-halo term dominates), and therefore a lower clustering at those scales.

because subhaloes are located within host systems of typical sizes $\lesssim 1\ h^1$ Mpc. Therefore, the addition of orphan galaxies, which are satellites, will enhance the clustering at small scales (Kitzbichler & White 2008).

The fraction of satellite haloes with respect to total (satellites + centrals) for the SMDPL simulation is 0.152, while for MDPL2 this fraction is 0.122. This indicates that we have roughly 25 percent more satellite haloes with masses between $10^{10.4} - 10^{12}\ h^{-1}\,\mathrm{M}_\odot$ in SMDPL than in MDPL2. Therefore, we conclude that the discrepancy observed between the two-point correlation functions of these simulations at small scales (see Figure 2) is due to the greater fraction of satellite haloes in SMDPL compared to MDPL2. To compensate for this lack of low-mass subhaloes we introduce the orphan galaxies, integrating their orbits until they merge with their host halo (see Section 2).

These additional satellite galaxies will modify both the HMF and the 2PCF at small scales. Comparing these functions in SMDPL and MDPL2 simulations, and assuming that their differences could be solved by following in a semi-analytic way the dynamics of those subhaloes that will host orphan galaxies, we find a way to constrain the parameters of the orbit model for such satellites.

3.3 Calibration volumes

The goal is to make a fast exploration of the parameters of the orbit model, to find regions of the parameter space where there is convergence between the simulations (i.e., similar HMF and 2PCF) after applying the orbit model. Since running the model over the full simulations is computationally very expensive, we are interested in finding a set of boxes that are relatively small in volume but representative of the characteristics of the full simulations. We consider sub-volumes with the following box sizes: SMDPL 50 h^{-1} Mpc, MDPL2 50 h^{-1} Mpc and MDPL2 100 h^{-1} Mpc. In addition, when selecting these sub-volumes we need to estimate their "goodness" (in the sense that they reproduce the characteristics of the full simulations). Here, we exemplify how to obtain the best box for MDPL2 50 h^{-1} Mpc; the other cases are analogous.

We begin partitioning MDPL2 into 8000 (20^3) disjoint subsamples with a box size of 50 h^{-1} Mpc. For each of these boxes, we calculate both ϕ and ξ. In the case of the correlation function ξ, we consider only haloes with masses greater than $10^{10.4}\ h^{-1}\,\mathrm{M}_\odot$, i.e. where the MDPL2 simulations is complete. Using these results, we compute the mean values of the HMFs and the 2PCFs, $\overline{\phi}$ and $\overline{\xi}$, respectively. Analogously, we obtain the mean values $\overline{\phi}$ and $\overline{\xi}$ for both MDPL2 100 h^{-1} Mpc (with 10^3 subvolumes) and SMDPL 50 (with 8^3 subvolumes).

Figures 3 and 4 show (in circle-dashed line) the mean values for the HMF and 2PCF, respectively. We also plot (in continuos line) the HMF and 2PCF corresponding to the full simulations. For both figures, we have the following cases: SMDPL 50 h^{-1} Mpc (left), MDPL2 50 h^{-1} Mpc (centre) and MDPL2 100 h^{-1} Mpc (right). Error bars indicate the standard deviation of the subvolume sets. In Figure 3, we note that, as it happens in the MDPL2 full simulation, the boxes also present a lack of low mass haloes (centre and right). The vertical dashed line indicates the minimum mass we consider in our study ($10^{10.4}\ h^{-1}\ \mathrm{M}_\odot$). Figure 4 shows the clustering signal computed considering only haloes with masses greater than $10^{10.4}\ h^{-1}\,\mathrm{M}_\odot$. We note that for very low separations ($\lesssim 0.02\ h^{-1}$ Mpc), the scatter in ξ is high, which is reflected in the magnitude of the error bars. This effect is mainly due to the fact that at these scales, the number of pairs is scarce and therefore Poissonian error dominates.

In order to find the best MDPL2 50 h^{-1} Mpc box, we need to characterise how representative each of our subsamples is. To estimate how much each box deviates from the full MDPL2 simulation (regarding to the 2PCF and the HMF), and pre-select some boxes that can be good candidates, we compute MAPE (mean absolute percentage error) estimates, i.e., for a given sub-box j, we compute the sum over all bins

$$\mathrm{MAPE}\left[h^{(j)}\right] = \frac{1}{n}\sum_{i=1}^{n}\frac{|h_i^{(j)} - h_i|}{|h_i|}, \tag{15}$$

where h represents either of the relevant constraining functions (i.e., the 2PCF ξ or the HMF ϕ), j indicates the given sub-box, and n is the number of bins where the function is computed. In this expression, h_i indicates the value of function h in a given bin i corresponding to the full simulations.

As mentioned above, the full MDPL2 simulation is not complete for low masses; furthermore, the correlation function computed in boxes becomes too noisy for scales below 0.02 h^{-1} Mpc. Taking this into account, for each box we only consider MAPE $[\phi]$ errors for masses higher than $10^{10.4}\ h^{-1}\ M_\odot$ and MAPE $[\xi]$ errors for separations in the range $0.02 - 1\ h^{-1}$ Mpc. We choose candidates for the best MDPL2 50 h^{-1} Mpc box as the ones that simultaneously

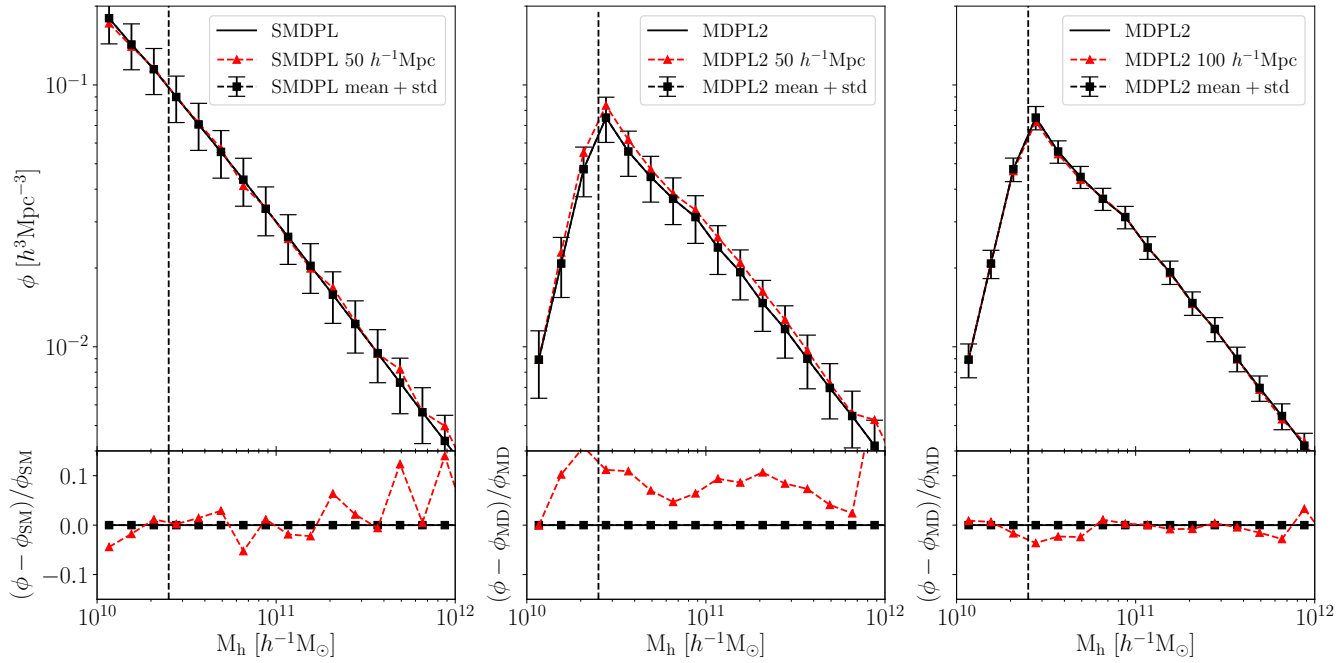

Figure 3. HMF for the selected boxes compared to the full simulations and the mean of the boxes. Results are shown for the SMDPL 50 h^{-1} Mpc (left), MDPL2 50 h^{-1} Mpc (centre) and MDPL2 100 h^{-1} Mpc (right). *Upper panels:* The continuos black line correspond to the full simulations. The circle-dashed black line shows the mean value for the halo mass function computed from the small boxes. The error bars correspond to the standard deviation at each halo mass bin. Red triangle-dashed lines correspond to the best boxes found. *Lower panels:* Fractional differences in HMF taking the full simulations as a reference. The vertical line denotes the mass cut at $\sim 10^{10.4}$ h^{-1} M$_\odot$. In the case of MDPL2 50 h^{-1} Mpc, the HMF of the selected box is slightly higher than the mean for all masses.

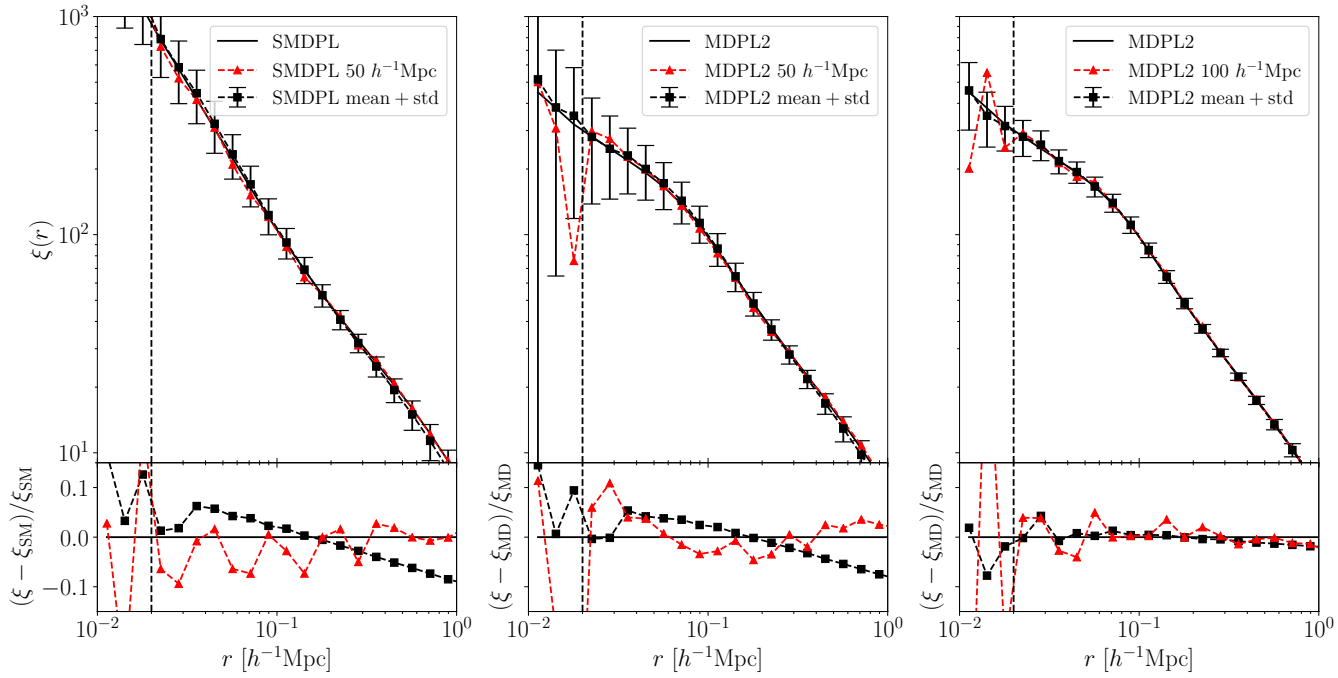

Figure 4. 2PCF for the selected boxes compared to the full simulations and the mean of the boxes. Results are shown for the SMDPL 50 h^{-1} Mpc (left), MDPL2 50 h^{-1} Mpc (centre) and MDPL2 100 h^{-1} Mpc (right). *Upper panels:* The continuous black line shows the mean value for the 2PCF computed from the small boxes. The error bars correspond to the standard deviation. Red dashed lines correspond to the best boxes found. *Lower panels:* Fractional differences in 2PCF taking the full simulations as a reference. The vertical dashed line indicates the scale 0.2 h^{-1} Mpc. This limit corresponds to the smaller scale we use to make the comparison, since below this limit, boxes have very few pairs and the correlation function becomes too noisy.

minimises both MAPE [ϕ] and MAPE [ξ]. From these candidates we choose our final best box by visual inspection, prioritizing the 2PCF.

Figure 3 shows in triangle-dashed red line the HMF of the best subvolumes for SMDPL 50 h^{-1} Mpc (left), MDPL2 50 h^{-1} Mpc (center) and MDPL2 100 h^{-1} Mpc (right). The method applied to find the best subvolumes for SMDPL 50 h^{-1} Mpc and MDPL2 100 h^{-1} Mpc, is analogous to what we have done for MDPL2 50 h^{-1} Mpc. Likewise, Figure 4 shows in triangle-dashed red lines the 2PCF of the best subvolumes for the same box sizes. These figures show that we are able to find smaller boxes in which to perform the parameter exploration, that are representative of the complete simulation boxes.

4 RESULTS

In this section, we make an exploration of the parameter space of the orbit model for orphan galaxies and see how the HMF and the 2PCF change when these parameters are varied. We recall the meaning of the parameters under consideration: b characterises the dynamical friction through the Coulomb logarithm (equation 4), α controls the tidal stripping (equation 6) and f is related to the merger criterion (equation 7).

Figure 5 shows the results obtained after applying the orbit model for orphan satellites to the MDPL2 50 h^{-1} Mpc sub-volume introduced in Section 3. Here we plot fractional differences taking the full SMDPL simulation as a reference, and selecting all haloes with masses greater than $10^{10.4}$ h^{-1} $M_\odot$ at redshift $z = 0$. The top panels show fractional differences in HMF while the bottom panels show fractional differences in 2PCF. The solid (black) line indicates the fractional difference between MDPL2 and SMDPL full simulations, while the dotted (black) line indicates the fractional difference for the MDPL2 50 h^{-1} Mpc box. The dashed lines with symbols correspond to fractional differences considering different parameter combinations of the model. In all panels, the dashed-circle (black) line correspond to the same parameters ($b = 0.35$, $f = 0.04$, $\alpha = 1.0$). From left to right we vary b (left panels), f (centre panels) and α (right panels), in each case we leave the remaining parameters fixed.

4.1 Variation of parameter b

The parameter b enters the dynamical friction force term through the Coulomb logarithm (see equations 1 and 4). Decreasing b is equivalent to increasing the value of the Coulomb logarithm $\ln\Lambda$ and this leads to a greater deceleration of subhaloes due to dynamical friction drag. Since decreasing b leads to a greater deceleration force, then we have a greater number of subhalo mergers and a lower number of total subhaloes. On the other hand, increasing b decreases the value of $\ln\Lambda$, we have smaller deceleration and the subhaloes decay at a slower rate. Thus, if we increase b we have a lower number of mergers and a greater number of total subhaloes.

As we have seen in the previous paragraph, decreasing b results in a smaller number of total subhaloes, and ϕ decreases over the entire mass range. On the other hand, if we increase b we have a greater number of total subhaloes and ϕ increases. The HMF for different values of b, it is shown in the upper-left panel of Figure 5. The 2PCF for different values of b is shown in dashed lines in the lower-left panel of Figure 5. Since increasing b results in a lower number of total satellite haloes, we have a smaller fraction of satellite haloes and the clustering signal decreases mainly at low scales. If we decrease b, we obtain a greater fraction of satellite haloes and the clustering increases at low scales. Note that since decreasing b implies that the satellite haloes decay faster, one might think there should be an increase in clustering at lower scales. However, this does not occur because most of these haloes end up merging with its main system and therefore do not contribute to the 2PCF.

4.2 Variation of parameter f

The parameter f is related to the merger criterion, increasing (decreasing) the value of f reduces (increases) the distance at which satellites merge with their hosts. Therefore, a higher value of f implies shorter merging times, a greater number of subhalo mergers and a lower number of total satellite haloes. A lower value of f implies larger merging times, a smaller number of mergers and a higher number of total satellite haloes.

The central panels of Figure 5 shows, in dashed lines, the results of the satellite model for different values of parameter f. As we have seen, a higher value of f implies a lower number of satellites haloes and the HMF decreases, while a lower value of f implies a higher number of total satellite haloes and the HMF increases. This is shown in the upper-central panel of Figure 5. For the 2PCF, we note that increasing (decreasing) f decreases (increases) the value of the correlation function ξ. This is shown in the lower-central panel of Figure 5. This effect is more relevant for separations below $\log(r/h^{-1}\mathrm{Mpc}) \leq -1$ than at intermediate separations, i.e. $\log(r/h^{-1}\mathrm{Mpc}) \geq -1$. Since increasing f decreases the number of satellite haloes, then we have a stronger clustering signal at low scales than for intermediate scales, because the 1-halo term of ξ depends strongly on the satellite fraction.

4.3 Variation of parameter α

The parameter α controls the rate at which the tidal stripping mechanism removes mass from a subhalo. A greater value of α implies a more efficient tidal stripping, and more material is removed via TS. A lower value of α slows down the TS effect and we have less material removed from a satellite.

The top-right panel of Figure 5 shows (in dashed lines) the HMF for different values of α. As we increase α, the HMF decreases over the entire range of masses. Since α controls the rate at which the tidal stripping mechanism removes mass from a subhalo, then a greater value of α implies a more efficient TS, and ϕ decreases. Finally, the bottom-right panel of Figure 5 shows (in dashed lines) the 2PCF for different values of α. Since increasing α increases the efficiency of TS, this reduces the fraction of satellite haloes and then the clustering signal decreases.

4.4 Best fitting parameters

To find the best fit parameters, we perform an exploration of the parameter space running the model over the calibration box MDPL2 50 h^{-1} Mpc varying the parameters b, f and α. For parameter b, we consider values in the range $0.05 - 1.50$, we allow f to vary between $0.01 - 0.08$ and α takes values between $1.0 - 5.0$. For each run output, we compute the corresponding HMF and the 2PCF at redshift $z = 0$ and then we compare the values of these functions with those of SMDPL. Then, we select the best fit parameters as those parameters that minimise the errors for HMF and 2PCF. The most suitable parameters found with this method corresponds to ($b = 0.02$, $f = 0.04$, $\alpha = 1.43$).

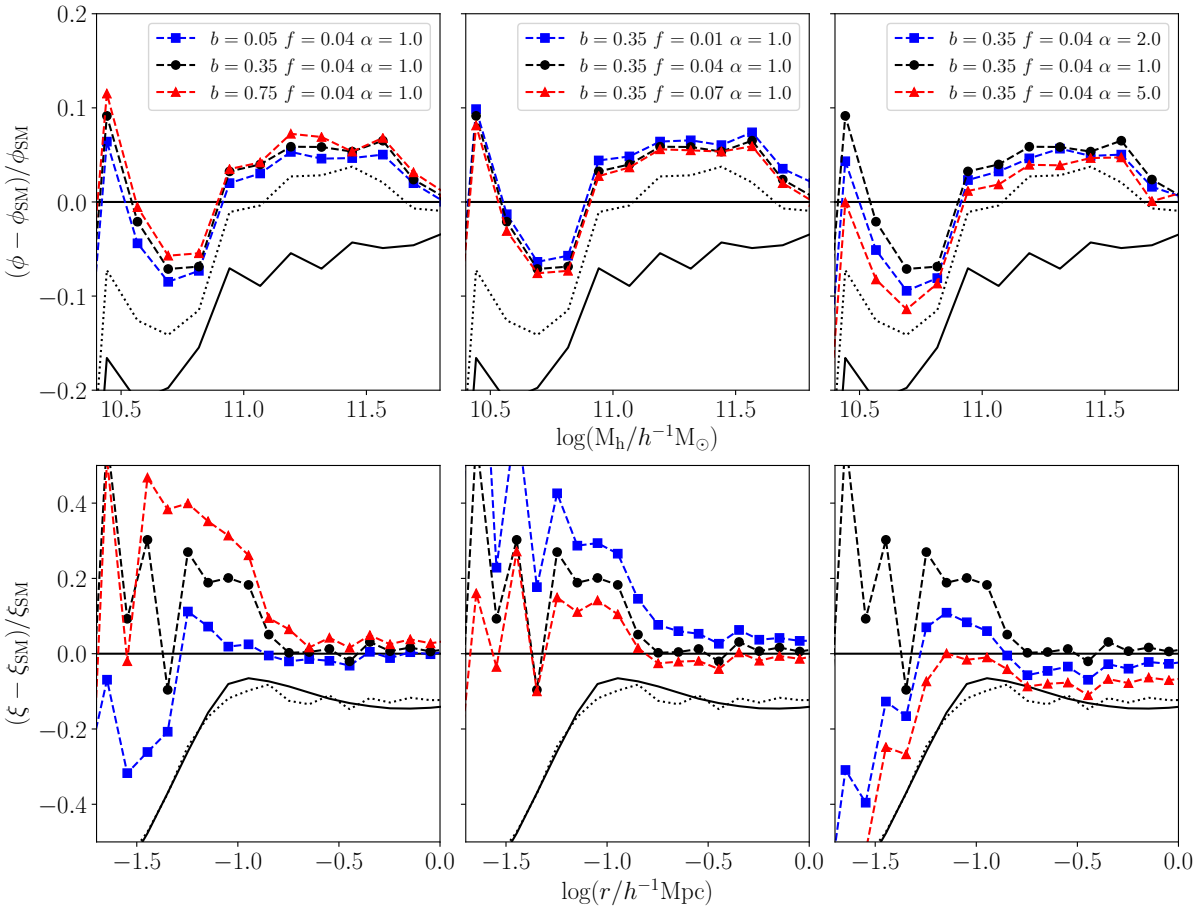

Figure 5. Fractional differences in HMF (top panels) and in 2PCF (bottom panels) with respect to the SMDPL full simulation for a sample obtained from applying the orbit model of orphan satellites to the MDPL2 50 h^{-1} Mpc calibration considering different parameter combinations of the model (dashed lined with symbols). The dashed-circle (black) line correspond to the same parameters ($b = 0.35$, $f = 0.04$, $\alpha = 1.0$) in all panels. Solid and dotted lines correspond to the fractional difference for MDPL2 and the MDPL2 50 h^{-1} Mpc calibration box, respectively. *Left panels:* effect of varying the parameter b leaving f and α fixed. Parameter b enters the dynamical friction force term through the Coulomb logarithm. Decreasing this parameter increases $\ln\Lambda$ and the DF effect, thus more satellite merge with its host and ϕ decreases. Since we have a smaller satellite fraction, the clustering signal ξ also decreases. *Central panels:* correspond to different values of the parameter f leaving b and α fixed. The value of f determines the minimum distance a satellite halo can be from its host before it is considered as merged with it. Increasing this parameter, implies a higher number of mergers and a lower number of satellite haloes. This also impacts the clustering signal ξ, which decreases. *Right panels:* show the effect of varying α leaving b and f fixed. Increasing the value of α implies greater efficiency of the TS process and greater mass loss and, consequently, a lower number of satellite haloes. As we have fewer satellites, then ξ and ϕ decreases. For more details see text.

5 DISCUSSION

We present the treatment for the evolution of the orbits of orphan satellites and the method used for calibrating the free parameters of the model. Here we discuss in more detail some aspects of our results.

From the analysis presented above we have that, in general, the inclusion of the subhaloes of orphan galaxies helps to enhance the HMF over the entire mass range. However, as we can see from the panels upper-panels of Figure 5, HMF depends more strongly on parameter α, while varying b and f has little impact on the overall shape of the HMF. Since b and f are related mainly to the evolution of the position of the satellites, thus HMF fails to put a tight constraint on those parameters. In particular, note that since the dynamical friction decelaration is proportional to the mass of the satellite (equation 1), then massive haloes are more sensitive to variations of the DF model. However, the lack of massive subhaloes makes it difficult to put a strong constraint on parameter b using only information from the halo mass function.

On the other hand, we see that the 2PCF is sensitive to variations of the three parameters (see lower panels of Figure 5), although the behavior is different depending on the scales considered. For very small scales ($\lesssim 0.3\ h^{-1}$ Mpc, see van den Bosch et al. 2013), the correlation function is dominated by the 1-halo term which depends strongly on the satellite fraction, then this region is very sensitive to variations on the dynamical friction model (b) or the merging criterion (f). At greater separations ($\gtrsim 0.3\ h^{-1}$ Mpc), the 2-halo term begins to compete with the 1-halo term and the constraining power of the correlation function is reduced. It is worth noticing that if the strength of TS is high ($\alpha \sim 5.0$), then the clustering is strongly suppressed at small scales. This shows that while HMF fails to constraint b and f, the correlation function has great constraining power for all parameters of the model.

As a result of the exploration of the model parameters, we have found the following best fit: $b = 0.2$, $f = 0.04$, $\alpha = 1.43$. For

$b = 0.2$, we can estimate the maximum and minimum values of the Coulomb logarithm. Since the dynamical friction term can only produce deceleration, we impose that $\ln\Lambda = 0$ when $r \leq bR_{\rm sat}$, as in equation 4. On the other hand, in our simulations, the virial radius of haloes (and subhaloes) are in the range $10-1000\,h^{-1}$ kpc. Assuming a maximum satellite-host distance of the order of the virial radius of main systems, then we have that, at most, $r/R_{\rm sat} \sim R_{\rm vir}/R_{\rm sat} \sim 100$. Therefore, $(\ln\Lambda)_{\rm max} \sim 6.2$. These estimated values are in agreement with our simulations, where the maximum and minimum values for Coulomb logarithm are in the range $0 - 7.2$.

In the literature, there are previous works that explore the possible values that the Coulomb logarithm can take. Pullen et al. (2014) assume a fixed value $\ln\Lambda = 2$. Other authors choose the value of this parameter in order to reproduce the results of numerical simulations. For example, Velazquez & White (1999), by studying orbits in numerical simulations, find values of this parameter between $1 - 2$. On the other hand, Yang et al. (2020), using a model similar to the one presented here, perform a parameter space exploration finding values for $\ln\Lambda$ of the order of 1.5. Clearly, the maximum for Coulomb logarithm we have found does not agree with the results of these previous works. However, we remark that those results were obtained assuming a constant value for $\ln\Lambda$, whereas in our simulations we assume a Coulomb logarithm that varies with the satellite-host distance.

The parameter f determines the minimum distance a satellite can approach before merging with its host, therefore this value gives us an estimate of the size of the central galaxy that will inhabit the DM halo as provided by a SAM. For $f = 0.04$, the central galaxy size would be of the order $R_{\rm g} \sim 0.04R_{\rm vir}$. This value is compatible with the size-virial radius relation found by Kravtsov (2013). This relation links the half mass radius of a galaxy with the virial radius of its host according to $r_{1/2} \sim 0.02 - 0.03\,R_{200}$.

As we have seen, the parameter α controls the efficiency of TS mechanism. Zentner & Bullock (2003) assumes a fixed value $\alpha = 1$, while other authors adjust α in order to match the results of simulations finding $\alpha = 2.5$ (Zentner et al. 2005, Z05) and $\alpha = 3.5$ (Pullen et al. 2014, P14). On the other hand, other authors assume TS to be an instantaneous process which implies $\alpha = \infty$ (Peñarrubia & Benson 2005). In our parameter exploration, we have found that $\alpha = 1.43$, which is much smaller than the results obtained by Z05 and P14. Finally, our results suggest that a value $\alpha > 5$ would make the 2PCF to be almost totally suppressed at small separations, disfavouring an instantaneous tidal stripping scenario.

One possible explanation for our lower value of α, as compared to other works, could be the fact that in our model, the $\ln\Lambda$ is variable, whereas in previous works, this value is usually taken as constant. In our model, we initially have a larger value of $\ln\Lambda$, and hence, the satellites decay more rapidly and come closer to the host, where the TS is stronger. On the other hand, in the case of fixed $\ln\Lambda$, the initial deceleration is smaller and therefore it takes more time for the satellite to reach inner regions, where the density and TS are higher. To compensate for this, a higher value of α would be required, in order to have a higher mass loss.

We also perform a convergence test using the other calibration boxes described in Section 3.3. We run the model using the best fit parameters over MDPL2 050 h^{-1} Mpc (MD050), MDPL2 100 h^{-1} Mpc (MD100) and SMDPL 50 h^{-1} Mpc boxes (SM050). The results of this exercise are shown (in dashed lines with symbols) in Figure 6 and Figure 7 for HMF and 2PCF, respectively. In dotted lines with symbols we plot the calibration boxes without the orphan satellites. As a reference, we plot the MDPL2 full simulation (in dashed line) and the SMDPL full simulation (in continuous line). In the lower panel of these figures, we show fractional differences taking the SMDPL full simulation as a reference.

Figure 6 shows that, after applying the model, we have a good agreement on the different calibration boxes after including the orphan satellites (dashed lines with symbols), compared to the boxes without including the orphans (dotted lines with symbols). From this figure, we also notice that SMDPL 50 h^{-1} Mpc and MDPL2 50 h^{-1} Mpc present some "spikes" at masses of the order of $10^{12}\ h^{-1}\,{\rm M}_\odot$; this is a particular characteristic of the selected boxes. For lower halo masses, the inclusion of orphans in SMDPL 50 h^{-1} Mpc (in squares) has little impact on the halo mass function. For MDPL2 50 h^{-1} Mpc (in circles) we note that the addition of orphan satellites helps to enhance the HMF at low masses, in this case the agreement with the HMF of SMDPL full is within 5 percent over the entire mass range. Finally, for MDPL2 100 h^{-1} Mpc (in triangles), we obtain a good agreement (within 5 percent) with the other cases except for masses below $10^{11}\ h^{-1}\,{\rm M}_\odot$ where the difference is of the order of 10 percent.

Figure 7 shows the effect of running the model over the calibration boxes using the best fit parameters for the 2PCF. In general, the addition of orphan satellites in MDPL2 50 h^{-1} Mpc and MDPL2 100 h^{-1} Mpc, considerably improves the two point correlation function over the entire range of scales (dasehd lines with symbols), compared to the boxes without the addition of orphans (dotted lines with symbols). However, this enhancement is more important at small scales ($0.02 - 0.10\ h^{-1}$ Mpc) where the 1-halo term dominates, which mainly depends on the fraction of satellite haloes. In general, fractional errors for 2PCF are within 10 percent for the three cases considered. Note that for both MDPL2 subvolumes, the clustering is strongly suppressed with a discrepancy greater than 50 percent for scales close to $0.02\ h^{-1}$Mpc. From these results, we can conclude that the inclusion of orphans improves the HMF and 2PCF of the simulation with lower resolution (MDPL2) as compared to SMDPL.

With this analysis, we have shown that, on the one hand, the SMDPL simulation has a complete population of satellite galaxies above $10^{10.4}\ h^{-1}\,{\rm M}_\odot$, and can be used as a reference for the exploration of the parameters of the orbit model. Indeed, if we apply the orbit model to a smaller fraction of SMDPL, namely SMDPL 50 h^{-1} Mpc, we would obtain the same HMF and 2PCF (see Figure 6 and 7). On the other hand, the MDPL2 50 h^{-1} Mpc box is sufficiently good to test the parameters, and we do not need a larger box. This can be verified by taking a larger box, namely MDPL2 100 h^{-1} Mpc, in which the results, when the best fit parameters are used, are consistent with those of the MDPL2 50 h^{-1} Mpc box (the observed differences are due to the selected box).

6 CONCLUSIONS

In this paper, we present an updated model for the orbital evolution of dark matter subhaloes. The model used includes tidal stripping effects and dynamical friction. It also takes into account the possible merger of the haloes using a proximity criterion. We have characterised our model by three free parameters (b, f, α). The proposed model describes the main processes that affect the orbital evolution of a satellite halo and it is simple enough to be relatively cheap from a computational point of view (at least two order of magnitude faster than a full N-body simulation of the same resolution and size).

In order to calibrate the free parameters of the model, satellite halo evolution studies in the literature used the HMF as a constraint. Figure 5 shows that ϕ is sensitive to variations in the efficiency of the

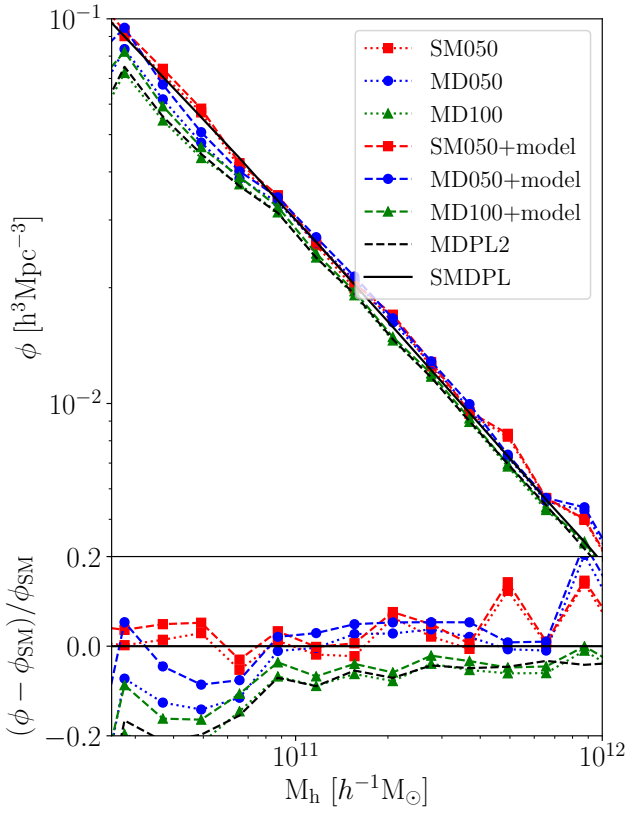

Figure 6. *Upper panel:* Halo mass functions. The dotted lines with symbols correspond to calibration boxes (see Section 3.3), i.e. without the orphan satellites. The dashed lines with symbols correspond to the calibration boxes after applying the orbit evolution model using the best parameters (see Section 4.4). Here SM050 correspond to SMDPL 50 h^{-1} Mpc best box, MD050 to MDPL2 50 h^{-1} Mpc and MD100 indicates 100 h^{-1} Mpc simulations. The simple dashed line denotes MDPL2 full and continuous line correspond to the SMDPL full simulation. *Lower panel:* Fractional differences taking the SMDPL full simulation as a reference. We see that after applying the model, for SMDPL 50 h^{-1} Mpc and MDPL2 50 h^{-1} Mpc the difference is below 5 percent for the entire mass range.

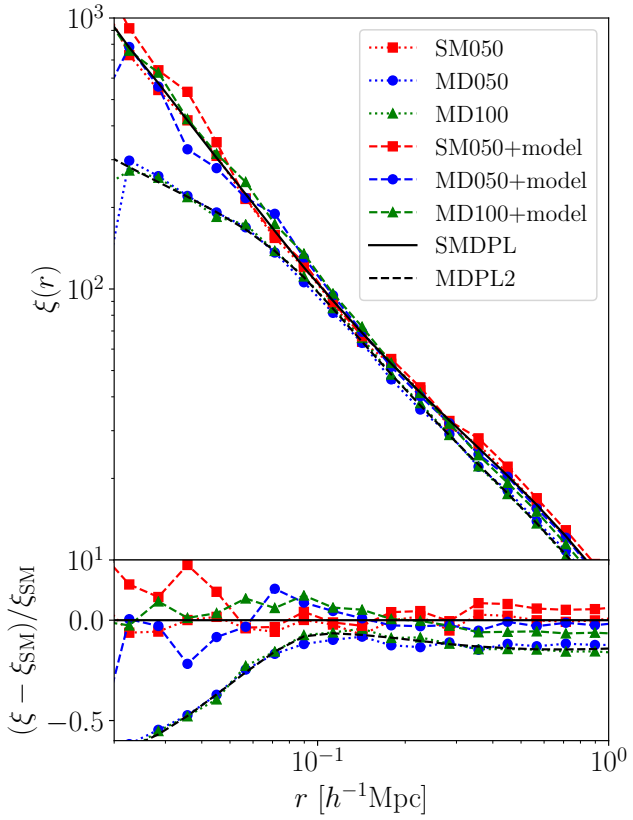

Figure 7. *Upper panel:* Two-point correlation functions. The dotted lines with symbols correspond to the calibration boxes, i.e. without the orphan satellites. The dashed lines with symbols correspond to the samples obtained from the best boxes after applying the orbit model using the best parameters. Here, SM050 correspond to SMDPL 50 h^{-1} Mpc best box, MD050 to MDPL2 50 h^{-1} Mpc and MD100 indicates MDPL2 100 h^{-1} Mpc satellites. The simple dashed line denotes MDPL2 full and continuous line correspond to the SMDPL full simulation. *Lower panel:* fractional differences in the HMFs taking SMDPL full as a reference. After applying the model, we obtain an enhancement of the clustering for MDPL2 50 h^{-1} Mpc and MDPL2 100 h^{-1} Mpc. In general, the agreement between the different calibration boxes is within 10 percent except for scales below 0.03 h^{-1} Mpc, where the agreement is within 20 percent.

tidal stripping (parameter α). On the other hand, the halo mass function fails to put tight constraints on the dynamical friction model, since this effect is most important for massive satellites, which are less abundant in the simulation (see right panels Figure 5). In this work, we have introduced the 2PCF as another constraint to the non-linear evolution of the orbits of orphan satellite haloes. In contrast with the HMF, the correlation function includes information about the distribution of subhaloes around their host. In this sense, the inclusion of clustering information helps to constrain the dynamical friction model and merging criterion (see left and centre panels of Figure 5).

We have performed an exploration of the parameter space of the model, this gives us the following best fit set ($f = 0.04, b = 0.02, \alpha = 1.43$). The value $f = 0.04$ is compatible with the value of half mass radius relation presented by Kravtsov (2013). The parameter b gives us a variable Coulomb logarithm which takes minimum - maximum values in the range $\ln\Lambda \sim 0 - 7.2$. Other works in the literature usually use $\ln\Lambda = 1 - 2$; since these values are taken to be constant, we cannot compare them directly with our results. On the other hand, $\alpha = 1.43$, the parameter that controls the efficiency of the TS mechanism, is lower compared to the values obtained in previous works. This might be related to the fact that we are assuming a variable Coulomb logarithm instead of a constant one, but this point requires further study.

Finally, we remark that we have not included a tidal heating term in our orbital evolution model. Tidal heating is a mechanism produced by rapid changes in tidal forces when a halo passes through the pericentre. These tidal shocks transfer energy to the satellite, then the subhalo expands and therefore a greater amount of matter is susceptible to be removed via tidal stripping. In a future work, we plan to include tidal heating effects in the orbital evolution of subhaloes and study individual orbits, taking special care on the evolution of masses and radius.

ACKNOWLEDGEMENTS

FMD and CGS are supported by the National Agency for the Promotion of Science and Technology (ANPCYT) of Argentina

grant PICT-2016-0081; and grants G140 and G157 from UNLP. CVM acknowledges support from ANID/FONDECYT through grant 3200918. SAC acknowledges funding from *Consejo Nacional de Investigaciones Científicas y Técnicas* (CONICET, PIP-0387), *Agencia Nacional de Promoción de la Investigación, el Desarrollo Tecnológico y la Innovación* (Agencia I+D+i, PICT-2018-03743), and *Universidad Nacional de La Plata* (G11-150), Argentina.

The CosmoSim database used in this paper is a service by the Leibniz-Institute for Astrophysics Potsdam (AIP). The MultiDark database was developed in cooperation with the Spanish MultiDark Consolider Project CSD2009-00064.

DATA AVAILABILITY

The data underlying this article will be shared on reasonable request to the corresponding author. The simulations used in this paper are publicly available at `https://www.cosmosim.org/`.

REFERENCES

Amendola L., et al., 2013, Living Reviews in Relativity, 16, 6
Baugh C. M., 2006, Reports on Progress in Physics, 69, 3101
Behroozi P. S., Conroy C., Wechsler R. H., 2010, ApJ, 717, 379
Behroozi P. S., Wechsler R. H., Wu H.-Y., 2013a, ApJ, 762, 109
Behroozi P. S., Wechsler R. H., Wu H.-Y., Busha M. T., Klypin A. A., Primack J. R., 2013b, ApJ, 763, 18
Benson A. J., 2010, Physics Reports, 495, 33
Benson A. J., 2012, New Astron., 17, 175
Berlind A. A., Weinberg D. H., 2002, ApJ, 575, 587
Berlind A. A., et al., 2003, ApJ, 593, 1
Binney J., Tremaine S., 2008, Galactic Dynamics: Second Edition
Boylan-Kolchin M., Ma C.-P., Quataert E., 2008, MNRAS, 383, 93
Brüggen M., De Lucia G., 2007, Monthly Notices of the Royal Astronomical Society, 383, 1336
Chandrasekhar S., 1943, ApJ, 97, 255
Coil A. L., 2013, The Large-Scale Structure of the Universe. p. 387, doi:10.1007/978-94-007-5609-0_8
Conroy C., Wechsler R. H., Kravtsov A. V., 2006, ApJ, 647, 201
Cooray A., Sheth R., 2002, Phys. Rep., 372, 1
Cora S. A., 2006, MNRAS, 368, 1540
Cora S. A., Muzzio J. C., Vergne M. M., 1997, MNRAS, 289, 253
Cora S. A., et al., 2018, ArXiv e-prints: 1801.03883,
Crain R. A., et al., 2015, MNRAS, 450, 1937
Croton D. J., et al., 2006, MNRAS, 365, 11
DESI Collaboration et al., 2016, arXiv e-prints, p. arXiv:1611.00036
Dawson K. S., et al., 2015, preprint, (`arXiv:1508.04473`)
Dawson K. S., et al., 2016, AJ, 151, 44
Euclid Collaboration et al., 2019, arXiv e-prints, p. arXiv:1910.09273
Frenk C. S., White S. D. M., 2012, Annalen der Physik, 524, 507
Gan J., Kang X., van den Bosch F. C., Hou J., 2010, Monthly Notices of the Royal Astronomical Society, 408, 2201
Gargiulo I. D., et al., 2015, MNRAS, 446, 3820
Gonzalez-Perez V., Lacey C. G., Baugh C. M., Lagos C. D. P., Helly J., Campbell D. J. R., Mitchell P. D., 2014, MNRAS, 439, 264
Gunn J. E., Gott J. Richard I., 1972, ApJ, 176, 1
Guo Q., White S., 2014, MNRAS, 437, 3228
Hashimoto Y., Funato Y., Makino J., 2003, ApJ, 582, 196
Henriques B. M. B., White S. D. M., Thomas P. A., Angulo R. E., Guo Q., Lemson G., Springel V., 2013, MNRAS, 431, 3373
Jenkins A., et al., 1998, ApJ, 499, 20
King I., 1962, AJ, 67, 471
Kitzbichler M. G., White S. D. M., 2008, Monthly Notices of the Royal Astronomical Society, 391, 1489
Klypin A., Yepes G., Gottlöber S., Prada F., Heß S., 2016, MNRAS, 457, 4340
Kravtsov A. V., 2013, ApJ, 764, L31
Kravtsov A. V., Berlind A. A., Wechsler R. H., Klypin A. A., Gottlöber S., Allgood B. o., Primack J. R., 2004, ApJ, 609, 35
LSST Dark Energy Science Collaboration 2012, arXiv e-prints, p. arXiv:1211.0310
LSST Science Collaboration et al., 2009, arXiv e-prints, p. arXiv:0912.0201
Lagos C. D. P., Cora S. A., Padilla N. D., 2008, MNRAS, 388, 587
Landy S. D., Szalay A. S., 1993, ApJ, 412, 64
Laureijs R., et al., 2011, preprint, (`arXiv:1110.3193`)
Levi M., et al., 2013, preprint, (`arXiv:1308.0847`)
Łokas E. L., Mamon G. A., 2001, MNRAS, 321, 155
Marinacci F., et al., 2018, MNRAS, 480, 5113
Martínez V. J., Saar E., 2001, Statistics of the Galaxy Distribution. Chapman and Hall/CRC, Boca Raton, FL, USA
Moster B. P., Somerville R. S., Maulbetsch C., van den Bosch F. C., Macciò A. V., Naab T., Oser L., 2010, ApJ, 710, 903
Muñoz Arancibia A. M., Navarrete F. P., Padilla N. D., Cora S. A., Gawiser E., Kurczynski P., Ruiz A. N., 2015, MNRAS, 446, 2291
Naiman J. P., et al., 2018, MNRAS, 477, 1206
Navarro J. F., Frenk C. S., White S. D. M., 1997, ApJ, 490, 493
Nelson D., et al., 2018, MNRAS, 475, 624
Ogiya G., Burkert A., 2016, MNRAS, 457, 2164
Orsi Á., Padilla N., Groves B., Cora S., Tecce T., Gargiulo I., Ruiz A., 2014, MNRAS, 443, 799
Peñarrubia J., Benson A. J., 2005, MNRAS, 364, 977
Peacock J. A., Smith R. E., 2000, MNRAS, 318, 1144
Peebles P. J. E., 1980, The large-scale structure of the universe
Petts J. A., Gualandris A., Read J. I., 2015, MNRAS, 454, 3778
Petts J. A., Read J. I., Gualandris A., 2016, MNRAS, 463, 858
Pillepich A., et al., 2018, MNRAS, 475, 648
Planck Collaboration et al., 2016, A&A, 594, A13
Pujol A., et al., 2017, MNRAS, 469, 749
Pullen A. R., Benson A. J., Moustakas L. A., 2014, ApJ, 792, 24
Reddick R. M., Wechsler R. H., Tinker J. L., Behroozi P. S., 2013, ApJ, 771, 30
Roukema B. F., Quinn P. J., Peterson B. A., Rocca-Volmerange B., 1997, MNRAS, 292, 835
Schaye J., et al., 2015, MNRAS, 446, 521
Silk J., Mamon G. A., 2012, RAA, 12, 917
Sinha M., Garrison L. H., 2020, MNRAS, 491, 3022
Springel V., 2005, MNRAS, 364, 1105
Springel V., Yoshida N., White S. D. M., 2001a, New Astron., 6, 79
Springel V., White S. D. M., Tormen G., Kauffmann G., 2001b, MNRAS, 328, 726
Springel V., et al., 2018, MNRAS, 475, 676
Taylor J. E., Babul A., 2001, ApJ, 559, 716
Tecce T. E., Cora S. A., Tissera P. B., Abadi M. G., Lagos C. D. P., 2010, MNRAS, 408, 2008
The LSST Dark Energy Science Collaboration et al., 2018, arXiv e-prints, p. arXiv:1809.01669
Tinker J., Kravtsov A. V., Klypin A., Abazajian K., Warren M., Yepes G., Gottlöber S., Holz D. E., 2008, ApJ, 688, 709
Trujillo-Gomez S., Klypin A., Primack J., Romanowsky A. J., 2011, ApJ, 742, 16
Vale A., Ostriker J. P., 2004, MNRAS, 353, 189
Vargas-Magaña M., et al., 2013, A&A, 554, A131
Velazquez H., White S. D. M., 1999, MNRAS, 304, 254
Vogelsberger M., Marinacci F., Torrey P., Puchwein E., 2020, Nature Reviews Physics, 2, 42
Vollmer B., Cayatte V., Balkowski C., Duschl W. J., 2001, ApJ, 561, 708
Wechsler R. H., Tinker J. L., 2018, ARA&A, 56, 435
Weinberg M. D., 1986, ApJ, 300, 93
White S. D. M., Rees M. J., 1978, MNRAS, 183, 341
Yang S., Du X., Benson A. J., Pullen A. R., Peter A. H. G., 2020, MNRAS, 498, 3902
Zentner A. R., Bullock J. S., 2003, ApJ, 598, 49

Zentner A. R., Berlind A. A., Bullock J. S., Kravtsov A. V., Wechsler R. H., 2005, ApJ, 624, 505
eBOSS Collaboration et al., 2020, arXiv e-prints, p. arXiv:2007.08991
van den Bosch F. C., More S., Cacciato M., Mo H., Yang X., 2013, MNRAS, 430, 725

APPENDIX A: INGREDIENTS OF THE ORBIT MODEL FOR A NFW DENSITY PROFILE

In numerical studies, the detected dark matter haloes are well described by a double power-law function of the radius, first introduced by (Navarro et al. 1997). Here we describe the Navarro-Frenk-White (NFW) density profile, and we give expressions for the dynamical friction formula and tidal radius equation corresponding to this particular profile. The Navarro-Frenk-White is given by the following expression

$$\rho(r) = \frac{\rho_c^0 \delta_{\rm char}}{\frac{r}{r_s}\left(1+\frac{r}{r_s}\right)^2}. \tag{A1}$$

The parameters of this expression are the scale radius r_s and the characteristic density $\delta_{\rm char}$. The concentration parameter is defined as

$$c = \frac{r_{\rm vir}}{r_s}, \tag{A2}$$

where $r_{\rm vir}$ is the virial radius of the halo, defined as the distance from the center of the halo within which the mean density is Δ times the critical density ρ_c^0. The value of the virial overdensity is often assumed to be 178, predicted by the spherical collapse model. However, numerical simulations typically use $\Delta = 200$.

We also introduce the dimensionless distance s and the function $g(c)$, which often appears in calculations involving the NFW profile,

$$s = \frac{r}{r_{\rm vir}}, \tag{A3}$$

$$g(c) = \frac{1}{\log(1+c) - c/(1+c)}. \tag{A4}$$

With the above definitions, the density equation becomes

$$\frac{\rho(s)}{\rho_c^0} = \frac{\Delta c^2 g(c)}{3s(1+cs)^2}. \tag{A5}$$

The mass of the halo is usually defined as the mass within the virial radius

$$M_{\rm vir} = \frac{4}{3}\pi r_{\rm vir}^3 \Delta \rho_c^0 \tag{A6}$$

Then the mass profile in units of the virial mass is

$$\frac{M(s)}{M_{\rm vir}} = g(c)\left[\log(1+cs) - \frac{cs}{1+cs}\right] \tag{A7}$$

Using the same definitions, we can express the gravitational potential as

$$\frac{\Phi(s)}{V_c^2} = -g(c)\frac{\log(1+cs)}{s}, \tag{A8}$$

where V_c^2 is the circular velocity at $r = r_{\rm vir}$.

For a point particle moving within a halo with a NFW density profile, the i-component of the acceleration is

$$\mathbf{a} = -g(c)\left[\frac{\log(1+cs)}{s^2} - \frac{c}{(1+cs)s}\right]\frac{\mathbf{s}}{s} \tag{A9}$$

In this case, the Chandrasekhar formula for the dynamical friction force is given by

$$\mathbf{a}_{\rm df} = -\frac{M_{\rm sat}\ln\Delta_c}{v^2}\frac{c^2 g(c)}{s(1+cs)^2}\left[{\rm erf}(X) - \frac{2X}{\sqrt{\pi}}{\rm exp}{-X^2}\right]\frac{\mathbf{v}}{v}. \tag{A10}$$

Finally, we need to compute the tidal radius, i.e.

$$r_t = \left(\frac{GM_{\rm sat}}{\omega^2 - d^2\Phi/dr^2}\right)^{1/3}. \tag{A11}$$

For $d^2\Phi/dr^2$ we have

$$\frac{d^2\Phi}{dr^2}(r = r_{\rm sat}) = -\frac{2GM_{\rm host}(< r_{\rm sat})}{r_{\rm sat}^3} + 4\pi G\rho(r_{\rm sat}). \tag{A12}$$

Then using the above expressions for $M_{\rm host}$ (A7) and $\rho_{\rm host}$ (A5), we obtain the tidal radius.

This paper has been typeset from a TEX/LATEX file prepared by the author.